A Three-Dimensional Analysis of Rotordynamic Forces on Whirling and Cavitating Helical Inducers

Luca d'Agostino
Associate Professor,
Università degli Studi di Pisa, Pisa, Italy

Fabrizio d'Auria
ESA Post-Doctoral Scholar,
California Institute of Technology,
Pasadena, CA 91125

Christopher E. Brennen
Professor,
Division of Engineering and
Applied Science,
California Institute of Technology,
Pasadena, CA 91125

This paper investigates the linearized dynamics of three-dimensional bubbly cavitating flows in helical inducers. The purpose is to understand the impact of the bubble response on the radial and tangential rotordynamic forces exerted by the fluid on the rotor and stator stages of whirling turbomachines under cavitating conditions. The flow in the inducer annulus is modeled as a homogeneous inviscid mixture, containing vapor bubbles with a small amount of noncondensable gas. The effects of several contributions to the damping of the bubble dynamics are included in the model. The governing equations of the inducer flow are written in "body-fitted" orthonormal helical Lagrangian coordinates, linearized for small-amplitude perturbations about the mean flow, and solved by modal decomposition. The whirl excitation generates finite-speed propagation and resonance phenomena in the two-phase flow within the inducer. These, in turn, lead to a complex dependence of the lateral rotordynamic fluid forces on the excitation frequency, the void fraction, the average size of the cavitation bubbles, and the turbopump operating conditions (including, rotational speed, geometry, flow coefficient and cavitation number). Under cavitating conditions the dynamic response of the bubbles induces major deviations from the noncavitating flow solutions, especially when the noncondensable gas content of the bubbles is small and thermal effects on the bubble dynamics are negligible. Then, the quadratic dependence of rotordynamic fluid forces on the whirl speed, typical of cavitation-free operation, is replaced by a more complex behavior characterized by the presence of different regimes where, depending on the whirl frequency, the fluid forces have either a stabilizing or a destabilizing effect on the inducer motion. Results are presented to illustrate the influence of the relevant flow parameters.

1 Introduction

The combined effects of destabilizing rotordynamic fluid forces and cavitation represent the main fluid dynamic phenomena that adversely affect the dynamic stability and performance of high power density turbopumps (Brennen, 1994). This can lead to very serious problems ranging from fatigue failure to sudden destructive damage of the machine (Jery et al., 1985; Franz et al., 1990). Rotordynamic fluid forces under cavitating conditions have long been known to play an important role in promoting the development of self-sustaining lateral motions (whirl) of the impeller (Rosenmann, 1965). Recent experiments carried out in the Rotor Force Test Facility at the California Institute of Technology by Franz et al. (1990) and Bhattacharyya (1994) showed that cavitation significantly affects the rotordynamic fluid forces on axial flow inducers. In general, cavitation has been found to have a destabilizing effect on the whirl motion. In the present context, it is important to note that cavitation replaces the characteristic quadratic behavior of the noncavitating rotordynamic fluid forces with a more complex dependence on the whirl speed, thereby undermining the traditional expansion of the rotordynamic fluid forces in terms of stiffness, damping and inertia matrices. Bhattarcharyya (1994) tentatively correlated these changes to the development of reverse (possibly oscillatory) flow at lower flow coefficients, implicitly postulating some form of interaction between cavitation, backflow and whirl motion.

The present research aims at obtaining some fundamental understanding of the basic fluid dynamic phenomena responsible for the observed behavior of the rotordynamic fluid forces in whirling and cavitating inducers. In particular, the main purpose of this study consists of investigating to what extent this behavior results from the dynamic response of the bubbles in the cavitating flow through the inducer under the excitation provided by the whirl motion. The flow is studied using the linear perturbation approach used by the authors in their previous dynamic analyses of bubbly liquids (d'Agostino and Brennen, 1983, 1988, 1989; d'Agostino, Brennen and Acosta, 1988; Kumar and Brennen, 1993; d'Auria, d'Agostino and Brennen, 1994, 1996), extending earlier two-dimensional results (d'Auria, d'Agostino and Brennen, 1995) to account for the presence of the inducer blades and the occurrence of significant tangential components of the rotordynamic fluid forces. By introducing suitable simplifications, this approach leads to a fully three-dimensional boundary value problem for a linear Helmholtz equation in the complex amplitude of the pressure perturbation. Solution to this equation can be efficiently obtained by separation of variables. Despite its intrinsic limitations, the results of the theory are consistent with the general features of the available experimental data. Hence, it appears that the present analysis correctly captures some of the fundamental fluid dynamic phenomena in whirling inducers under cavitating conditions and can usefully contribute to the understanding of the rotordynamic fluid forces and instabilities in a number of important turbomachinery applications.

Contributed by the Fluids Engineering Division for publication in the JOURNAL OF FLUIDS ENGINEERING. Manuscript received by the Fluids Engineering Division January 21, 1998; revised manuscript received May 5, 1998. Associate Technical Editor: J. Katz.

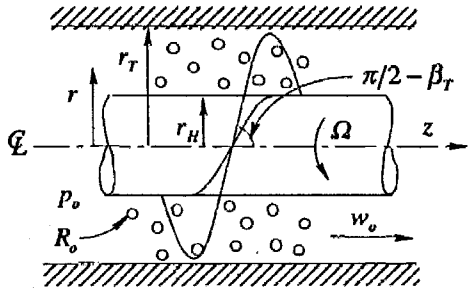

Fig. 1 Schematic of the flow configuration and inducer geometry

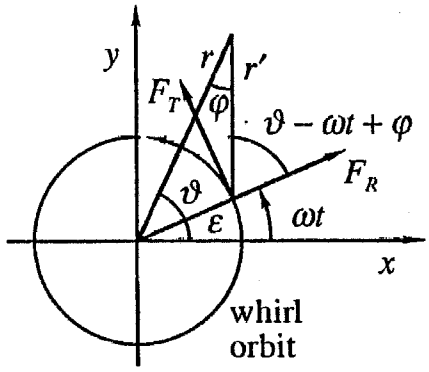

Fig. 2 Schematic of whirl motion, coordinates and rotordynamic forces

2 Linearized Dynamics of a Bubbly Flow in a Whirling Impeller

We address the problem of the flow of an incompressible liquid of velocity $\mathbf{u}$, pressure p, and density, ρ_L, in a helical inducer rotating with velocity, Ω, and whirling on a circular orbit of small eccentricity, ϵ, at angular speed, ω. We define an absolute (inertial) system of cylindrical coordinates (r, ϑ, z), fixed on the axis of the duct surrounding the inducer, and relative cylindrical coordinates, (r', ϑ', z'), fixed in the impeller, as illustrated in Figs. 1 and 2. Hence, to the first order in the eccentricity, the coordinate transformation is:

$$r = r' - \epsilon \cos(\vartheta - \omega t),$$

$$\vartheta' = \vartheta - \Omega t + \frac{\epsilon}{r}\sin(\vartheta - \omega t) \quad \text{and} \quad z' = z$$

A number of simplifying assumptions are introduced in order to obtain a soluble set of equations that still reflects the dynamics of a whirling inducer in a bubbly mixture. The relative motion of the two phases, whose dynamic role is insignificant in the present linearized approximation (d'Agostino and Brennen, 1989), is neglected. Viscous effects are also neglected, except in the bubble dynamics where they contribute to the damping. As shown in Fig. 1, an infinite helical inducer is considered, with N radial blades, zero blade thickness, hub radius r_H, tip radius r_T, tip blade angle β_T, and constant pitch:

$$P = 2\pi r_T \tan\beta_T = 2\pi r' \tan\beta$$

The mean flow conditions are specified by the flow coefficient, ϕ, and the cavitation number, σ, assuming fully-guided forced-vortex flow with axial velocity $w_o = \phi\Omega r_T$, angular velocity $\Omega_o = \Omega(1 - \phi \cot\beta_{oT})$, zero radial velocity u_o, and uniform mean pressure $p_o = p_{Vo} + \sigma\rho_L\Omega^2 r_T^2/2$ (neglecting centrifugal effects), where p_{Vo} is the vapor pressure of the liquid.

Cavitation is modeled by a uniform distribution of small spherical bubbles of unperturbed radius, R_o, and void fraction, $\alpha \ll 1$. The dynamics of vapor-gas bubbles is modeled as proposed by Nigmatulin et al. (1981), assuming uniform internal pressure, equal gas and vapor temperatures, and linear subsonic bubble oscillations. For assigned values of the pressure, temperature, and surface tension of the surrounding liquid it is possible to determine the amount of non-condensable gas stabilizing a bubble of given radius (d'Auria et al., 1997). The effects of compressibility, inertia, and energy dissipation due to the viscosity of the liquid and the transfer of heat and mass between the two phases are included in the model. In this model, the vapor-gas bubbles, when excited at frequency ω_L, behave as second-order harmonic oscillators:

$$(-\omega_L^2 - i\omega_L 2\lambda + \omega_B^2)\hat{R} = -\frac{\hat{p}}{\rho_L R_o} \tag{1}$$

where $\hat{R}$ and $\hat{p}$ are the complex amplitudes of the bubble radius and liquid pressure perturbations:

$$\tilde{R} = R - R_o = \mathrm{Re}\{\hat{R}\exp(-i\omega_L t)\} \quad \text{and}$$

$$\tilde{p} = p - p_o = \mathrm{Re}\{\hat{p}\exp(-i\omega_L t)\}.$$

Assuming that the gas and vapor densities are negligible when compared to the liquid density and solving the energy equation at $R = R_o$, the damping coefficient $\lambda = \lambda(\omega_L)$ and the bubble natural frequency $\omega_B = \omega_B(\omega_L)$ are obtained as:

Nomenclature

a = sound speed
b = boundary equation
$\mathbf{e}$ = unit vector
E = bubble thermodynamic function
F = force
i = imaginary unit
j = blade index
J = Bessel function of the first kind
k = wave number, thermal conductivity
l = hub excitation mode index
m = blade excitation mode index
n = cross-flow helical coordinate
N = number of blades
p = pressure
P = blade axial pitch
r = radial coordinate
R = bubble radius
s = streamwise helical coordinate
t = time
$\mathbf{u}$ = velocity vector
u, v, w = velocity components
x, y, z = Cartesian coordinates
Y = mass fraction, Bessel function of the second kind
α = void fraction
β = blade angle
γ = specific heat ratio
ϵ = whirl eccentricity
ϑ = azimuthal coordinate
λ = bubble damping coefficient
μ = eigenvalue
ν = kinematic viscosity
ρ = density
σ = cavitation number
τ = bubble volume
φ = angle
ϕ = flow coefficient
ω = frequency, whirl angular speed
Ω = rotational speed

Subscripts and Superscripts

B = bubble, blade
G = gas
H = hub
I = inducer
L = liquid, Lagrangian
M = bubbly mixture
p = pressure
R = radial
T = tangential, blade tip
v = volume
V = vapor
VG = vapor-gas mixture
o = unperturbed or reference value

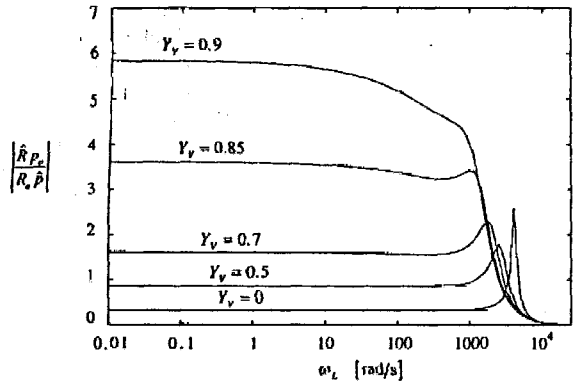

Fig. 3 "Cold bubble." Radius response, $|\hat{R}p_o/R_o\hat{p}|$, of a 1 mm radius gas-vapor bubble in water at $p_o = 5 \cdot 10^3$ Pa, $T_o = 293$ K, as a function of the excitation frequency, ω_L, for different values of the bubble vapor content: $Y_v = 0$ (noncondensable gas bubble), $Y_v = 0.5$, $Y_v = 0.7$, $Y_v = 0.85$, and $Y_v = 0.9$ (from d'Auria et al., 1997).

$$2\lambda = \frac{3p_{Bo}}{\rho_L R_o^2 \omega_L} \operatorname{Im}\left\{\frac{\gamma_{VG}}{E(\omega_L)}\right\} + \frac{4\nu_L}{R_o^2} \tag{2}$$

$$\omega_B^2 = \frac{3p_{Bo}}{\rho_L R_o^2} \operatorname{Re}\left\{\frac{\gamma_{VG}}{E(\omega_L)}\right\} - \frac{2S}{\rho_L R_o^3} \tag{3}$$

which are similar to the expressions of Chapman and Plesset (1972) and Prosperetti (1984, 1991). Here γ_{VG} is the specific heat ratio of the vapor-gas mixture inside the bubble, ν_L and S are the kinematic viscosity and the surface tension of the liquid, and $p_{Bo} = p_o + 2S/R_o$ is the bubble internal pressure, which is the sum of the partial pressure of the vapor, p_{Vo}, and of the non-condensable gas, p_{Go}. The quantity $E = E(\omega_L)$ accounts for the bubble compressibility, interfacial phase changes, heat transfer, mass diffusion, and inertial effects (Nigmatulin et al., 1981).

It is important to note that the dynamic behavior of vapor-gas bubbles changes dramatically when the temperature is such that interfacial heat transfer limits the bubble dynamics (Brennen, 1995). This is illustrated in Figs. 3 and 4, where the response of bubbles with different vapor content is plotted as a function of the excitation frequency for $p_o = 5000$ and 40,000 Pa, respectively corresponding to temperatures of 20° and 70° Celsius. In both cases the normalized amplitude of the bubble response increases rapidly with the vapor content. However, vapor-gas bubbles at 20°C are much more compliant than those

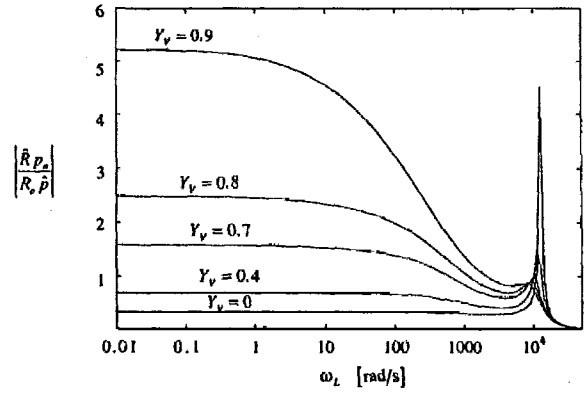

Fig. 4 "Warm bubble." Radius response, $|\hat{R}p_o/R_o\hat{p}|$, of a 1 mm radius gas-vapor bubble in water at $p_o = 4 \cdot 10^4$ Pa, $T_o = 343$ K, as a function of the excitation frequency, ω_L, for different values of the bubble vapor content: $Y_v = 0$ (noncondensable gas bubble), $Y_v = 0.4$, $Y_v = 0.7$, $Y_v = 0.8$, and $Y_v = 0.9$ (from d'Auria et al., 1997).

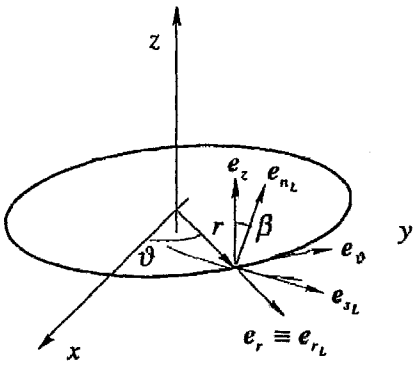

Fig. 5 Schematic of the transformation from the cylindrical coordinates r, ϑ, z to the orthogonal helical coordinates r_L, s_L, n_L

at 70°C. This has important consequences for the forces acting on the inducer.

The perturbation velocities must satisfy the kinematic conditions on the hub, $D(r' - r_H)/Dt = 0$, on the outer casing, $D(r - r_T)/Dt = 0$, and on the blade:

$$\frac{D}{Dt}\left\{\vartheta' + \frac{z'}{r_T}\cot\beta_T - \vartheta_j'\right\} = 0$$

where $\vartheta_j' = 2\pi(j-1)/N$ identifies the angular position of the jth blade ($j = 1, 2, \ldots N$). It is convenient to analyze the flow in body-fitted Lagrangian helical coordinates:

$$r_L = r, \quad s_L = \frac{\vartheta - \Omega_o t}{2\pi}\cos^2\beta - \frac{z - w_o t}{P}\sin^2\beta,$$

$$n_L = \frac{N}{2\pi}(\vartheta - \Omega_o t) + \frac{N}{P}(z - w_o t)$$

moving with the mean flow at axial velocity, w_o, and angular speed, Ω_o, and normalized so that s_L and n_L are incremented by 1 for one rotation about the axis (see Fig. 5). Then, the linearized kinematic conditions for the Lagrangian velocity perturbations $(\tilde{u}, \tilde{v}, \tilde{w})$ on the solid surfaces are found to be:

$$\tilde{u} = \epsilon\omega_L \sin\left(2\pi s_L + \frac{2\pi}{N} n_L \sin^2\beta - \omega_L t\right)$$

on the hub $\quad r_L = r_H$

$$\tilde{u} = 0 \quad \text{on the casing} \quad r_L = r_T$$

and:

$$\tilde{w} = \epsilon\frac{P\omega_L\cos\beta}{2\pi r_L}\cos\left(2\pi s_L + \frac{2\pi}{N} n_L \sin^2\beta - \omega_L t\right)$$

on the blades $\quad n_L = 1, 2, \ldots N$

where $\omega_L = \omega - \Omega_o$ is the frequency of the bubble excitation in the Lagrangian frame. Finally, appropriate boundary conditions at the inlet and exit of the inducer are needed. Here, for simplicity, we impose periodic conditions $\tilde{p}(s_L) = \tilde{p}(s_L + 1)$, consistent with the original assumption that the inducer is long in the axial direction.

Generalizing the derivation of d'Agostino and Brennen (1988), linearization of the fluid dynamic equations of the bubbly mixture in rotating coordinates for time-harmonic fluctuations with frequency ω_L and irrotational absolute velocity perturbations yields the following Helmholtz equation for the pressure field:

$$\nabla^2\hat{p} + k^2(\omega_L)\hat{p} = 0 \tag{4}$$

where the free-space wave number, k, is determined using the principal branch of the complex square root from the dispersion relation:

$$\frac{1}{a_M^2(\omega_L)} = \frac{k^2(\omega_L)}{\omega_L^2} = \frac{1}{a_{Mo}^2}\left(\frac{\omega_{Bo}^2}{\omega_B^2 - \omega_L^2 - i\omega_L 2\lambda}\right)$$

Here $a_M(\omega_L)$ is the complex (dissipative) and dispersive (frequency dependent) speed of propagation of harmonic disturbances of angular frequency, ω_L, in the free bubbly mixture, and a_{Mo} is the low-frequency sound speed, given by:

$$a_{Mo}^2 = \frac{\omega_{Bo}^2 R_o^2}{3\alpha(1-\alpha)}$$

where $\omega_{Bo}^2 = \omega_B^2(0)$ is the natural frequency of oscillation of a single bubble at isothermal conditions ($\omega_L \to 0$) in an unbounded liquid. Assuming uniform mean pressure in the inducer, k is constant and, neglecting Coriolis forces ($\Omega_o \approx 0$), to this order of approximation, the complex velocity and pressure perturbations are related, as usual, by $i\omega_L\rho_L(1-\alpha)\hat{u} = \nabla\hat{p}$.

With the above boundary conditions, the homogeneous Helmholtz equation for the pressure represents a well-posed complex boundary value problem for $\hat{p}$. If the blade angle $\beta = \beta(r)$ is approximated by a constant value β_o at some suitable mean radius r_o, the separable solution (Lebedev, 1965) in the blade channel $j-1 \le n_L \le j$ is:

$$\hat{p} = \sum_{l=0}^{+\infty} a_l R_{Hl}(r_L)\cos[2\pi(n_L - j + 1)]e^{i(2\pi s_L - \omega_L t)} + \sum_{m=0}^{+\infty} R_{Bm}(r_L)\{c_{mj}\cos[\mu_m(n_L - j + 1)] - c_{mj-1}\cos[\mu_m(n_L - j)]\}e^{i(2\pi s_L - \omega_L t)} \tag{5}$$

where:

$$a_0 = \epsilon\rho_L(1-\alpha)\omega_L^2 r_H \int_{j-1}^{j} \exp\left(i\frac{2\pi}{N}n_L \sin^2\beta_o\right)dn_L$$

$$a_l = 2\pi l\epsilon\rho_L(1-\alpha)\omega_L^2 r_H \times \int_{j-1}^{j} \exp\left(i\frac{2\pi}{N}n_L \sin^2\beta_o\right)\cos[l\pi(n_L - j + 1)]dn_L \quad \text{for } l \neq 0$$

$$c_{mj} = \frac{\epsilon N\rho_L(1-\alpha)\omega_L^2}{i2\pi\mu_m \sin\mu_m} \frac{\int_{r_H}^{r_T} \exp\left(i\frac{2\pi}{N}j\sin^2\beta_o\right)R_{Bm}(r_L)dr_L}{\int_{r_H}^{r_T}\frac{N^2 r_L}{P^2\cos^2\beta_o}R_{Bm}^2(r_L)dr_L}$$

In these equations $R_{Hl}(r_L)$ and $R_{Bm}(r_L)$ are the modal solutions corresponding to the hub and blade excitation, given in terms of the Bessel functions of the first and second kind and order $\nu = \cos\beta_o$ by:

$$R_{Hl}(r_L) = \frac{1}{B_l r_H}\frac{J_\nu(B_l r_L)Y'_\nu(B_l r_T) - Y_\nu(B_l r_L)J'_\nu(B_l r_T)}{J'_\nu(B_l r_H)Y'_\nu(B_l r_T) - Y'_\nu(B_l r_H)J'_\nu(B_l r_T)}$$

$$R_{Bm}(r_L) = J_\nu(B_m r_L)Y'_\nu(B_m r_T) - Y_\nu(B_m r_L)J'_\nu(B_m r_T)$$

where B_m are the (infinite and positive) zeros of the equation:

$$J'_\nu(Br_H)Y'_\nu(Br_T) - Y'_\nu(Br_H)J'_\nu(Br_T) = 0$$

and B_l and μ_m are the principal square roots of:

$$B_l^2 = k^2(\omega_L) - \frac{l^2\pi^2 N^2}{P^2\cos^2\beta_o} \quad \text{and}$$

$$\mu_m^2 = \frac{P^2\cos^2\beta_o}{N^2}[k^2(\omega_L) - B_m^2]$$

In the presence of bubble dynamic damping, the series for $\hat{p}$ in Eq. (5) converges rapidly and only the first few terms are needed in the computations.

In the special case of no bubble dynamic damping, k^2 is real and the boundary value problem for $\hat{p}$ is self-adjoint with real eigenvalues, μ_m^2. If, in particular, $k^2 r_T^2 < \cos^2\beta_o$, then all eigenvalues μ_m^2 are negative. Given the functional dependence of the solution, this condition and the dispersion relation identify the cut-off frequency:

$$\omega_L^* = \omega^* - \Omega_o = \omega_{Bo}\Big/\left(1 + \frac{3\alpha(1-\alpha)r_T^2}{R_o^2\cos^2\beta_o}\right)^{1/2} \tag{6}$$

beyond which no wave-like propagation of the blade excitation takes place in the n_L-direction. From the above equations it also appears that resonance occurs in response to the hub and blade excitation when $B_l = B_m$ and $\mu_m = l\pi$, respectively. This leads to an infinite set of natural frequencies:

$$\omega_{Llm} = \omega_{lm} - \Omega_o = \omega_{Bo}\Big/\left(1 + \frac{3\alpha(1-\alpha)/R_o^2}{B_m^2 + l^2\pi^2 N^2/P^2\cos^2\beta_o}\right)^{1/2} \tag{7}$$

for $l > 0$, $m > 0$. Notice that, consistent with the results of previous dynamic analyses of bubbly flows (d'Agostino and Brennen, 1983, 1988, 1989; d'Agostino et al., 1988; d'Auria, d'Agostino and Brennen, 1994, 1995, 1996), ω_L^* and ω_{Llm} never exceed the resonance frequency ω_{Bo} of an individual bubble, and become much lower when a "cloud interaction" parameter, β, becomes significantly greater than unity. In the present case, $\beta = \alpha L^2/R^2$ where $L = r_T$.

The rotordynamic fluid force per unit length on the inducer is:

$$\mathbf{F} = -\frac{1}{\pi\epsilon P\rho_L\Omega^2 r_T^2}\int_{S_l}(p - p_o)d\mathbf{S} \tag{8}$$

where S_l is the surface of the inducer (hub and blade surfaces) for one interval $0 \le \vartheta \le 2\pi$.

Upon integration, the radial and tangential components, F_R and F_T, of the rotordynamic force on the inducer are more compactly represented in complex form by:

$$F = F_R - iF_T \tag{9}$$

Due to the linear nature of the solution, it is possible to synthesize the rotordynamic forces by examining the separate contributions from the hub and blade motion. With the notation of Eq. (9), the rotordynamic force on the hub generated by the hub motion is:

$$F^{(HH)} = F_R^{(HH)} - iF_T^{(HH)} = -\frac{1}{\pi\epsilon P\rho_L\Omega^2 r_T^2}\sum_{j=1}^{N}\sum_{l=0}^{+\infty}\frac{\pi P r_H}{N}a_l R_{Hl}(r_H)I_{lj} \tag{10}$$

where:

$$I_{lj} = \int_{j-1}^{j}\exp\left(-i\frac{2\pi}{N}n_L\sin^2\beta_o\right)\cos[l\pi(n_L - j + 1)]dn_L$$

Similarly, the rotordynamic force on the hub generated by the blade motion is:

$$F^{(HB)} = F_R^{(HB)} - iF_R^{(HB)} = -\frac{1}{\pi\epsilon P\rho_L\Omega^2 r_T^2} \times \sum_{j=1}^{N}\sum_{m=0}^{+\infty} \frac{\pi P r_H}{N} R_{Bm}(r_H)(c_{mj}A_{mj} - c_{mj-1}B_{mj}) \quad (11)$$

where:

$$A_{mj} = \int_{j-1}^{j} \exp\left(-i\frac{2\pi}{N} n_L \sin^2\beta_o\right) \cos\left[\mu_m(n_L - j + 1)\right] dn_L$$

$$B_{mj} = \int_{j-1}^{j} \exp\left(-i\frac{2\pi}{N} n_L \sin^2\beta_o\right) \cos\left[\mu_m(n_L - j)\right] dn_L$$

The complex representation of the rotordynamic force on the blades generated by the hub motion is:

$$F^{(BH)} = F_R^{(BH)} - iF_T^{(BH)} = \frac{1}{\pi\epsilon P\rho_L\Omega^2 r_T^2} \times \left\{ \sum_{j=1}^{N}\sum_{i=0}^{+\infty} i\frac{Pa_i}{2}\int_{r_H}^{r_T} R_{HI}(r_L) e^{-i(2\pi/N)(j-1)\sin^2\beta_o} dr_L - (-1)^i \sum_{j=1}^{N}\sum_{i=0}^{+\infty} i\frac{Pa_i}{2}\int_{r_H}^{r_T} R_{HI}(r_L) e^{-i(2\pi/N)j\sin^2\beta_o} dr_L \right\} \quad (12)$$

and, finally, the rotordynamic force on the blades generated by the blade motion is:

$$F^{(BB)} = F_R^{(BB)} - iF_T^{(BB)} = \frac{1}{\pi\epsilon P\rho_L\Omega^2 r_T^2} \times \left\{ \sum_{j=1}^{N}\sum_{m=0}^{+\infty} i\frac{P}{2}(c_{mj} - c_{mj-1}\cos\mu_m) \times \int_{r_H}^{r_T} R_{Bm} e^{-i(2\pi/N)(j-1)\sin^2\beta_o} dr_L - \sum_{j=1}^{N}\sum_{m=0}^{+\infty} i\frac{P}{2}(c_{mj}\cos\mu_m - c_{mj-1}) \times \int_{r_H}^{r_T} R_{Bm} e^{-i(2\pi/N)j\sin^2\beta_o} dr_L \right\} \quad (13)$$

Then, the rotordynamic forces on the inducer are simply synthesized as:

$$F = F_R - iF_T = F^{(HH)} + F^{(HB)} + F^{(BH)} + F^{(BB)} \quad (14)$$

The modes R_{HI}, due to the hub motion, are analogous to the earlier two-dimensional flow solution (d'Auria et al. 1995), except for relatively minor modifications introduced by the helical nature of the flow. These mostly contribute to the radial component of the rotordynamic force. On the other hand, the modes R_{Bm}, due to the blade motion are essentially three-dimensional and generate significant contributions to the tangential forces.

The entire flow has therefore been determined in terms of the material properties of the two phases, the geometry of the impeller, the nature of the excitation, and the assigned quantities ϕ, σ, α, and R_o.

3 Results and Discussion

The calculated rotordynamic forces acting on the inducer as a consequence of the whirl motion are strongly dependent on the propagation of pressure disturbances through the blade channels. The general features of this propagation (behavior in space and time, dependence on the flow parameters, resonances and cut-off frequencies, etc.) have already been examined (d'Auria et al., 1995) and will not be reviewed here in detail.

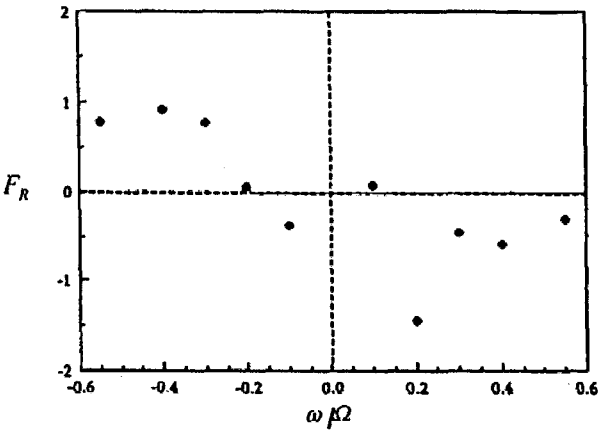

Fig. 6 Experimentally measured radial rotordynamic force on the test inducer as a function of the whirl speed ratio ω/Ω under cavitating conditions at $\phi = 0.049$ and $\sigma = 0.106$ (adapted from Bhattacharyya, 1994)

The rotordynamic fluid forces predicted by the present model will be compared with the experimental results obtained by Bhattacharyya (1994) for a helical inducer ($r_T = 5.06$ cm, $r_H/r_T = 0.4$, $\beta_T = 9°$, $\epsilon = 0.254$ mm) operating in water at $\Omega = 3000$ rpm with flow coefficients of $\phi = 0.049$ and $\phi = 0.074$ (not corrected for hub blockage) and different values of the cavitation number, σ.

Figures 6 and 7 show some typical experimental data at a flow coefficient, $\phi = 0.049$, and a cavitation number $\sigma = 0.106$. Notice that the forces do not vary quadratically with the whirl frequency, ω, and that their behavior is characterized by multiple zero crossings. The radial force (Fig. 6) is essentially negative for $\omega/\Omega > -0.2$, and has a minimum at $\omega/\Omega \cong 0.2$. Similar behavior was observed for other cavitation numbers (Bhattacharya, 1994). In the tangential forces (Fig. 7), the most interesting feature is the strong positive (destabilizing) peak at $\omega/\Omega \cong 0.2$. This peak was present in all of the experiments of Bhattacharyya (1994); it increased in magnitude as the cavitation number, σ, increased and the flow coefficient, ϕ, decreased.

Typical results for the radial and tangential rotordynamic forces predicted by the present theory for the same inducer at $\phi = 0.049$, and $\sigma = 0.106$ are displayed in Fig. 8 as a function of the whirl speed ratio ω/Ω. Despite the differences between

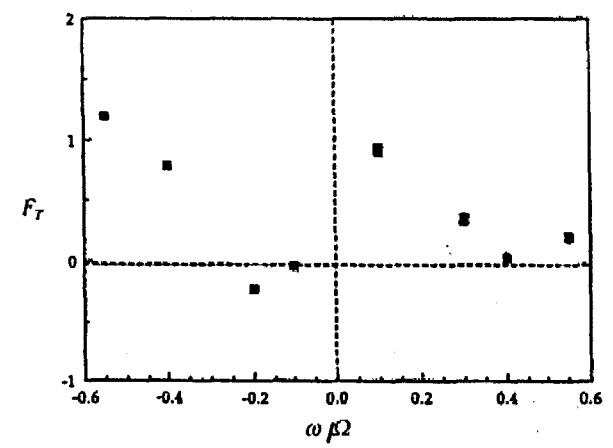

Fig. 7 Experimentally measured tangential rotordynamic force on the test inducer as a function of the whirl speed ratio ω/Ω under cavitating conditions at $\phi = 0.049$ and $\sigma = 0.106$ (adapted from Bhattacharyya, 1994)

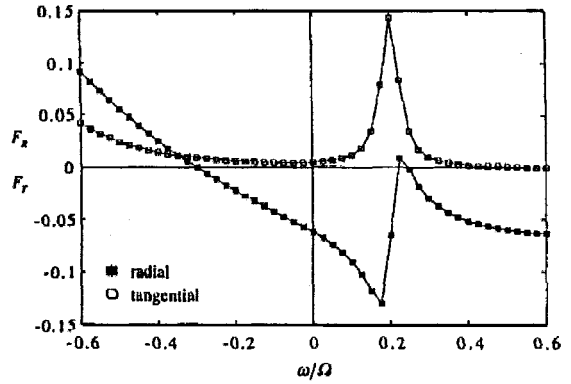

Fig. 8 Radial and tangential rotordynamic forces on the test inducer as a function of the whirl speed ratio ω/Ω under cavitating conditions at $\phi = 0.049$, $T_o \simeq 293$ K, $\alpha = 0.005$, $R/r_T = 0.01$, $p_o \simeq 2255$ Pa, and $Y_V \simeq 0.875$

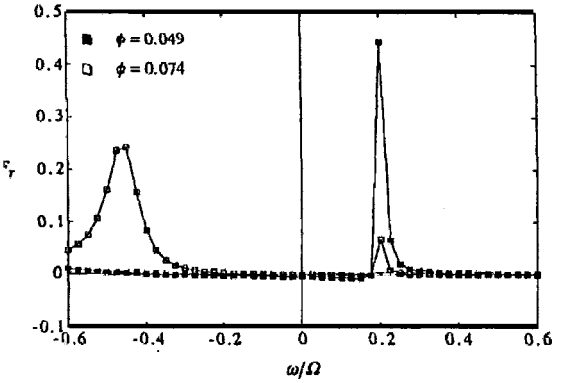

Fig. 10 Tangential rotordynamic force on the test inducer as a function of the whirl speed ratio ω/Ω under cavitating conditions at $\alpha = 0.03$, $T_o = 293$ K, $R/r_T = 0.01$, $p_o \simeq 2255$ Pa, for two different values of the flow coefficient, ϕ

theory and experiment (notice, for example, that the magnitude of the forces is off by one order of magnitude), the main qualitative features of the forces are correctly reproduced. Note that, consistent with experimental results, the radial force, F_R, is essentially negative for $\omega/\Omega > -0.3$. In addition, the zero crossing for positive whirl ratios and the minimum at $\omega/\Omega \approx 0.2$ have been reproduced by the computations. More important, in view of its implications for rotordynamic stability, Fig. 8 shows that the strong positive peak in the tangential force and its location ($\omega/\Omega \approx 0.2$) are also reproduced by the theory. Figure 9 presents results for various void fractions. As the void fraction increases, the magnitude of the peak in the tangential force increases. This is physically consistent with the experimental observations of Bhattacharyya (1994), who observed the same increase as the cavitation number, σ, decreased. Figure 10 presents results for various flow coefficients and demonstrates that a similar effect occurs as ϕ decreases.

These results are strongly influenced by bubble dynamics effects. The corresponding value of the cloud interaction parameter $3\alpha(1-\alpha)r_T^2/R_o^2$ (as defined by d'Agostino and Brennen, 1989) is much larger than unity, thus indicating that extensive bubble dynamic and resonant phenomena are likely to occur in the inducer flow.

Finally, we turn our attention to the influence of thermal effects on the rotordynamic forces. Figure 11 shows the behavior of the tangential force for different values of the temperature in the liquid. It may be observed that, as the temperature in the flow increases, the peak decreases in magnitude and eventually disappears. This behavior results from the different bubble response at different temperatures, as exemplified by Figs. 3 and 4.

A few brief remarks on the discrepancies between the present theory and experimental results are appropriate. First, the magnitude of the rotordynamic forces is systematically underestimated. A plausible cause for this discrepancy is the variation of cavitation in the radial direction in the blade channels. Also the (rather unrealistic) assumptions that all bubbles have the same radius and therefore the same resonant dynamic behavior results in more localized peaks than those observed. Finally, the present theory necessarily neglects the secondary flows that are inevitably present in cavitating inducers (Brennen, 1994).

4 Conclusions

The results of this study show that bubble dynamics cause major modifications of the rotordynamic forces on cavitating inducers.

The propagation of the whirl-induced disturbances within the inducer is significantly modified by the large reduction of the sonic speed in the bubbly cavitating flow. The spectral response of the rotordynamic fluid forces is strongly correlated to the cloud interaction parameter, $3\alpha(1-\alpha)r_T^2/R_o^2$, and the relative magnitude of the excitation and bubble resonance frequencies. Most of the paper focuses on cavitation that is uninhibited by thermal effects though we also demonstrate the damping effects introduced when thermal effects become important.

The computations show that the rotordynamic fluid forces on the inducer in bubbly cavitating flows no longer vary quadratically with the whirl frequency, as in noncavitating conditions.

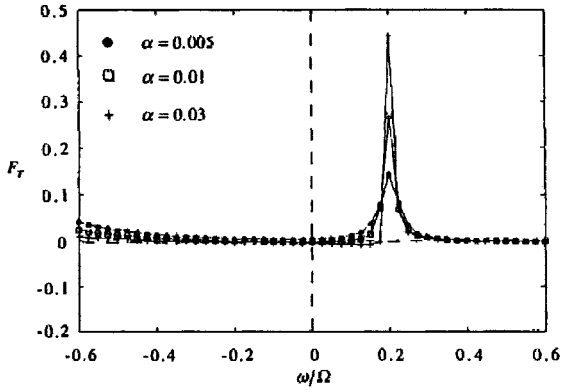

Fig. 9 Tangential rotordynamic force on the test inducer as a function of the whirl speed ratio ω/Ω under cavitating conditions at $\phi = 0.049$, $T_o = 293$ K, $R/r_T = 0.01$, $p_o = 2255$ Pa, for three different values of the void fraction, α

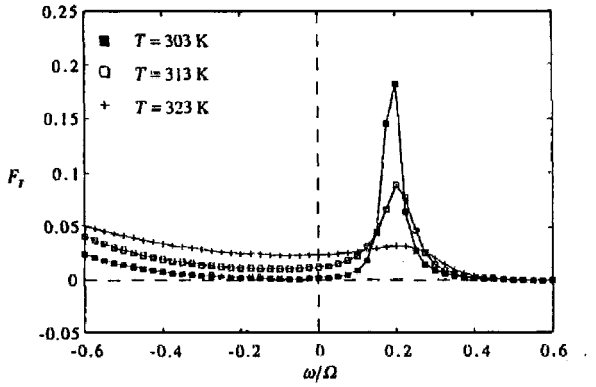

Fig. 11 Tangential rotordynamic force on the test inducer as a function of the whirl speed ratio, ω/Ω, under cavitating conditions at $\phi = 0.049$, $R_o/r_T = 0.007$, $p_L = 35000$ Pa, and three different temperature levels

The theory qualitatively reproduces the main characteristics of the rotordynamic forces (though there are significant quantitative discrepancies). In particular, the occurrence of a strong destabilizing peak in the tangential force is correctly predicted, including the frequency at which it occurs and the evolution of the magnitude with cavitation number and flow coefficient. These results provide the first real insight into the complex physical phenomena observed experimentally.

Acknowledgments

This research project was carried out on internal funds by CentroSpazio, Ospedaletto (Pisa) Italy, as well as under a European Space Agency External Post-Doctoral Fellowship. Financial support was also provided by a grant from the Foundation Blanceflor Boncompagni-Ludovisi, född Bildt. The authors would like to express their gratitude to Mr. Riccardo Marsili, undergraduate student at Pisa university, for carrying out most of the computations, to Prof. Mariano Andrenucci, Director of Centrospazio, and Prof. Renzo Lazzeretti of the Aerospace Engineering Department, University of Pisa, Pisa, Italy, for their friendly encouragement in the completion of the present work.

References

Bhattacharyya, A., 1994, "Internal Flows and Force Matrices in Axial Flow Inducers," Ph.D. thesis, Division of Engineering and Applied Science, California Institute of Technology, Pasadena, CA.

Brennen, C. E., 1994, *Hydrodynamics of Pumps*, Concepts ETI, Inc. and Oxford University Press.

Brennen, C. E., 1995, *Cavitation and Bubble Dynamics*, Oxford University Press.

Chapman, R. B., and Plesset, M. S., 1972, "Nonlinear Effects in the Collapse of a Nearly Spherical Cavity in a Liquid," ASME *Journal of Basic Engineering*, Vol. 94, pp. 172–183.

d'Agostino, L., and Brennen, C. E., 1988, "Acoustical Absorption and Scattering Cross-Sections of Spherical Bubble Clouds," *Journal of the Acoustical Society of America*, Vol. 84 (6), pp. 2126–2134.

d'Agostino, L., and Brennen, C. E., 1989, "Linearized Dynamics of Spherical Bubble Clouds," *Journal of Fluid Mechanics*, Vol. 199, pp. 155–176.

d'Agostino, L., Brennen, C. E., and Acosta, A. J., 1988, "Linearized Dynamics of Two-Dimensional Bubbly and Cavitating Flows over Slender Surfaces," *Journal of Fluid Mechanics*, Vol. 192, pp. 485–509.

d'Auria, F., d'Agostino L. and Brennen C. E., 1994, "Linearized Dynamics of Bubbly and Cavitating Flows in Cylindrical Ducts," ASME FED Vol. 194, pp. 59–66.

d'Auria F., d'Agostino L. and Brennen C. E., 1995, "Bubble Dynamic Effects on the Rotordynamic Forces in Cavitating Inducers," ASME FED Vol. 201, pp. 47–54.

d'Auria F., d'Agostino L., and Brennen C. E., 1996, "Dynamic Response of Ducted Bubbly Flows to Turbomachinery-Induced Perturbations," ASME JOURNAL OF FLUIDS ENGINEERING, Vol. 118, pp. 595–601.

d'Auria, F., d'Agostino, L., and Burzagli, F., 1997, "Linear Stability of Parallel Two-Dimensional Shear Layers Containing Vapor-gas Bubbles," ASME FEDSM, Vancouver, BC, June 22–26.

Franz, R., Acosta, A. J., Brennen, C. E., and Caughey, T. K., 1990, "The Rotordynamic Forces on a Centrifugal Pump Impeller in the Presence of Cavitation," ASME JOURNAL OF FLUIDS ENGINEERING, Vol. 112, pp. 264–271.

Jery, B., Brennen, C. E., Caughey, T. K., and Acosta, A. J., 1985, "Forces on Centrifugal Pump Impellers," *Second International Pump Symposium*, Houston, Texas, April 29–May 2.

Lebedev, N. N., 1965, *Special Functions and Their Applications*, Prentice Hall.

Nigmatulin, R. I., Khabeev, N. S., and Nagiev, F. B., 1981, "Dynamics, Heat and Mass Transfer of Vapor-Gas Bubbles in a Liquid," *International Journal of Mass Transfer*, Vol. 24(6), pp. 1033–1044.

Prosperetti, A., 1984, "Bubble Phenomena in Sound Fields: Part One," *Ultrasonics*, Mar., pp. 69–78.

Prosperetti, A., 1991, "The Thermal Behavior of Oscillating Gas Bubbles," *Journal of Fluid Mechanics*, Vol. 222, pp. 587–616.

Rosenmann, W., 1965, "Experimental Investigations of Hydrodynamically Induced Shaft Forces with a Three Bladed Inducer," *Proceedings of the ASME Symposium on Cavitation in Fluid Machinery*, pp. 172–195.